# Solvent Decompositions and Physical Properties of Decomposition Compounds in Li-Ion Battery Electrolytes Studied by DFT Calculations and Molecular Dynamics Simulations

**Ken Tasaki***

*MC Research and Innovation Center, Inc., Goleta, California 93117*

*Received: June 24, 2004; In Final Form: November 10, 2004*

The density functional theory (DFT) calculations have been performed for the reduction decompositions of solvents widely used in Li-ion secondary battery electrolytes, ethylene carbonate (EC), propylene carbonate (PC), dimethyl carbonates (DMC), ethyl methyl carbonate (EMC), and diethyl carbonate (DEC), including a typical electrolyte additive, vinylene carbonate (VC), at the level of B3LYP/6-311+G(2d,p), both in the gas phase and solution using the polarizable conductor calculation model. In the gas phase, the first electron reduction for the cyclic carbonates and for the linear carbonates is found to be exothermic and endothermic, respectively, while the second electron reduction is endothermic for all the compounds examined. On the contrary, in solution both first and second electron reductions are exothermic for all the compounds. Among the solvents and the additive examined, the likelihood of undergoing the first electron reduction in solution was found in the order of EC > PC > VC > DMC > EMC > DEC with EC being the most likely reduced. VC, on the other hand, is most likely to undergo the second electron reduction among the compounds, in the order of VC > EC > PC. Based on the results, the experimentally demonstrated effectiveness of VC as an excellent electrolyte additive was discussed. The bulk thermodynamic properties of two dilithium alkylene glycol dicarbonates, dilithium ethylene glycol dicarbonate (Li-EDC) and dilithium 1,2-propylene glycol dicarbonate (Li-PDC), as the major component of solid−electrolyte interface (SEI) films were also examined through molecular dynamics (MD) simulations in order to understand the stability of the SEI film. It was found that film produced from a decomposition of EC, modeled by Li-EDC, has a higher density, more cohesive energy, and less solubility to the solvent than the film produced from decomposition of PC, Li-PDC. Further, MD simulations of the interface between the decomposition compound and graphite suggested that Li-EDC has more favorable interactions with the graphite surface than Li-PDC. The difference in the SEI film stability and the behavior of Li-ion battery cycling among the solvents were discussed in terms of the molecular structures.

Side reactions involving solvent decompositions at the solid−electrolyte interface (SEI) and the physical properties of SEI films together critically affect the performance of Li-ion rechargeable batteries: the safety, the self-discharge, the power, the faradic efficiency, the cycle life, the irreversible capacity loss ($Q_{ir}$) during the first charge cycle, and others. Though the SEI at the cathode side is of no less importance, we focus on the SEI at the anode side in this work. Among these characteristics, $Q_{ir}$ is most affected by processes involving solvent decompositions and reactions with Li salts at SEI, the processes eventually leading to an SEI passivation film formation on the anode surface. Other characteristics such as the cycle life, the safety, and the self-discharge depend on the properties of the SEI film itself such as the thickness, the density, the cohesiveness, the solubility to the electrolyte, the adhesion to the graphite surface, and others. Despite the considerable efforts made in studying the SEI compositions, the film formation reactions, and the morphology in the past three decades,[1−29] the nature of SEI films and their formation mechanism still remain considerably unknown.

The previous reports have been divided roughly into two widely held views as the first step for SEI film formation: the solvent decomposition at the graphite surface[16,26−29] prior to the Li co-intercalation of solvents or the solvent co-intercalation into the graphite layer followed by solvent decomposition.[30−33] In either case, the reactivity of solvents at the anode−electrolyte interface seems the first and foremost characteristic to be examined in the formation of SEI films in which solvent decomposition products are the major components. This is the first part of this work. Once formed on the graphite surface, some SEI films are prone to dissolution into the electrolyte or unstable at elevated temperatures, exposing the graphite surface to the electrolyte for further decomposition of the solvent. In addition, the SEI film formation is known to be sensitive to the nature of graphite as well.[34−36] It is thus clear that the physical properties of SEI films and the interactions between the SEI film and the graphite also play important roles determining the formation and the quality of the SEI film. This is the second part of the work.

The SEI film formation differs significantly among the solvents. For example, an SEI film can be formed in an ethylene carbonate (EC) based electrolyte, while exfoliation of graphite occurs and no SEI is formed in the propylene carbonate (PC) based electrolytes.[2,20,24,31,35] However, PC can be a practical rechargeable battery electrolyte solvent when an additive such as vinylene carbonate (VC) is added to the electrolyte, since an SEI film is formed in the presence of VC.[37] It is believed that VC facilitates SEI film formation on a graphite surface. The search for such additives in forming an effective SEI film has

* E-mail: ken_tasaki@m-chem.com.

10.1021/jp047240b CCC: $30.25 
Published on Web 01/29/2005

been found to be not straightforward, mainly due to the lack of understanding of the SEI film formation mechanism, and has been a subject of intense research activity in recent years.[38−45] Thus, SEI film formation may be sensitive to a number of factors: the reactivity of the solvent, the physical properties of the film, and the interaction of the film with the graphite surface, given the same Li salt.

In addition, while a Li-ion battery can be cycled in an electrolyte using dimethyl carbonate (DMC) or ethyl methyl carbonate (EMC) as a solvent, this does not seem to be the case when a diethyl carbonate (DEC) based electrolyte is used.[46] This observation is less established than the well-known difference for the EC-based and the PC-based electrolytes and needs further work; yet, the decomposition behaviors of various electrolytes apparently differ in the first cycling, and the reason for the difference remains unclear. A model study on the decomposition products may help shed light on these differences in the behavior of SEI film formation.

Regarding the effect of VC on the SEI film formation, Zhang et al. have reported the thermodynamic potentials for various solvent reductions, including VC, using density functional theory (DFT) calculations.[47,48] Yet, their calculations did not explain the benefit of using VC as an effective additive. The reduction mechanism used in their calculations was based on the one-electron reduction mechanism. They also reported oxidation potentials for organic solvents.[49] Later, Wang et al. reported a comprehensive study on the effect of VC on the SEI film formation when PC is used as a solvent.[50] It was found that VC stabilizes the reduction ion-pair intermediate of PC, thus promoting reduction of PC to form SEI film materials. Still, the discussion was more focused on the one-electron reduction mechanism than the second electron reduction mechanism. From the experimental side, Aurbach et al. recently suggested that VC undergoes polymerization on the graphite surface, forming polyalkyl lithium carbonates preventing decomposition of solvents and salts at the SEI,[51] which has been supported by another study as well.[52]

Dey et al. originally proposed the two-electron reduction mechanism based on the component analysis of SEI films.[53] The two-electron reduction of EC along with lithium ions, for example, gives the following products which are a mix of gases and solids:

$$\mathrm{EC} + 2\mathrm{e}^- + 2\mathrm{Li}^+ \rightarrow \mathrm{C_2H_4}\,(\uparrow) + \mathrm{Li_2CO_3}\,(\downarrow) \qquad (1)$$

$$\mathrm{EC} + 2\mathrm{e}^- + 2\mathrm{Li}^+ \rightarrow \mathrm{LiOCH_2CH_2OLi}\,(\downarrow) + \mathrm{CO}\,(\uparrow) \qquad (2)$$

$$\mathrm{EC} + 2\mathrm{e}^- + 2\mathrm{Li}^+ \rightarrow \mathrm{LiCH_2CH_2OCO_2Li}\,(\downarrow) \qquad (3)$$

All the reduction products in eqs 1−3 have been either directly or indirectly identified.[6,35,54−57] On the other hand, one-electron reduction of EC yields a dilithium alkylene glycol carbonate:

$$2\mathrm{EC} + 2\mathrm{e}^- + 2\mathrm{Li}^+ \rightarrow (\mathrm{CH_2OCO_2Li})_2\,(\downarrow) + \mathrm{CH_2CH_2}\,(\uparrow) \qquad (4)$$

The products of one-electron reductions have been also observed.[11,46,58,59] It has been suggested that the one-electron reduction product, $(CH_2OCO_2Li)_2$, reacts with $H_2O$ to give $Li_2CO_3$.[56] Though this scenario is certainly plausible, a recent report by in situ gas analysis showed little evidence for the reaction.[46] In fact, Aurbach et al. investigated the dependence of the film components on the solvent concentration and observed $Li_2CO_3$ as a main product at a low EC concentration, while $(CH_2OCO_2Li)_2$ was the predominant product at a higher EC concentration.[55] This finding demonstrates that $Li_2CO_3$ is produced by more than the reaction of $(CH_2OCO_2Li)_2$ with $H_2O$. The two-electron mechanism is supported by other studies[6,7,26,60,61] as well, including the recent DFT calculations[62] on EC which supported the two-electron reduction proposed by Aurbach. In the first half of the study, we have performed DFT calculations for reduction decomposition of various solvents, including VC as an SEI film additive, based on the two-electron mechanism.

As to the difference between the EC and PC electrolytes in the SEI film formation behavior, exhaustive calculations on the reductive decomposition intermediates and the mechanism have been reported by Wang et al.[50,63] These calculations are the most extensive and the highest levels of calculations to date performed on these solvents. Yet, their calculations on reactivity did little to explain the sharp difference between these solvents in the behavior of SEI film formation, suggesting that the discussion on the reactivity alone has a limit in addressing the SEI problems. Likewise, the differences among DMC, EMC, and DEC are yet to be understood in terms of their reactivity only. No high-level computational study on reactivity has yet to be reported for the linear carbonate solvents which are important solvents for Li-ion battery electrolytes.

Recently, several models have been proposed to explain the differences among the solvents.[31,64,65] Ogumi and co-workers have proposed that co-intercalation of solvent with lithium ions is the first step for SEI film formation in PC-based electrolyte and without a film formation additive, co-intercalation of PC causes exfoliation of graphite, while co-intercalation of EC leads to buildup of SEI film formation.[31] This is similar to Besenhard's earlier co-intercalation model.[1,14,33] On the other hand, Aurbach et al. have suggested that the difference in the cohesiveness of the SEI film produced in an EC-based electrolyte from that in a PC-based electrolyte is responsible for the sharp contrast in the behaviors during the first recharge cycle of a Li-ion secondary battery in the two electrolytes.[64] Earlier, Ein-Eli proposed the so-called "sticky-finger model" to explain the disparity in the cycle behaviors among various carbonate electrolytes by attributing it to the differences among them in the interactions between the decomposition products of the linear carbonates and the graphite surface as well as the quality of the film such as "the compactness".[65] The latter two models[64,65] are based on the decomposition product's properties rather than the reactivity of the solvents.

The stability of SEI film has also been an important issue in Li-ion battery research. It directly affects the cycle life, the calendar life, and the safety of batteries, and intense efforts have been made to understand the relationship between SEI film and the calendar life or safety and also to improve SEI film to enhance these characteristics.[66−68] The adhesion of the film to graphite, the integrity of the film itself, and the solubility of the film to electrolyte all matter in the film stability, among other factors, where the thermodynamic properties may play a greater role than the kinetic process. Ein-Eli presented the key properties of SEI films as prerequisites: a good adhesion to the graphite, a low solubility to the electrolyte, a small electric conductivity, and a high $Li^+$ conductivity.[65]

In the second half of the study, we examined the physical properties of the decomposition products in order to further understand the quality of SEI film such as the bulk properties, the interactions with graphite, and the solubility to electrolyte at the molecular level. We used two model compounds, the dilithium alkylene glycol dicarbonates from reduction reaction of EC and PC, dilithium ethylene glycol dicarbonate, $(LiOCO_2-$

$CH_2)_2$, and dilithium 1,2-propylene glycol dicarbonate, $CH_3$-$CH(OCO_2Li)CH_2OCO_2Li$, respectively. Both products have been identified as the major components of SEI films in both solvents.[69] Despite a large number of reports on SEI films, little is understood on their solubility to the solvents, their adhesion to the graphite surface, and the temperature dependence of the film properties. On the other hand, the experimental study on the physical properties, preferably in situ, is challenging. We thus used computational tools, DFT calculations and molecular dynamics (MD) simulations.

## Calculations

The solvents and the additive studied for the reactivity of reduction decomposition included EC, PC, DMC, EMC, DEC, and VC. The geometries of the molecules were all optimized at the HF/6-31G(d) level. The first electron reduction energy ($E_1 = E_{11} + E_{12}$, $E_{11}$ being the electron affinity and $E_{12}$ being the ring opening and the isomerization energies) and the second electron reduction energy ($E_2$) for these compounds were predicted by single-point calculations at the B3LYP/6-311+G-(2d,p) level, with the geometry optimized at the HF/6-31G(d) level, in the following reduction schemes using EC as an example: In the case of the linear carbonates, no ring opening

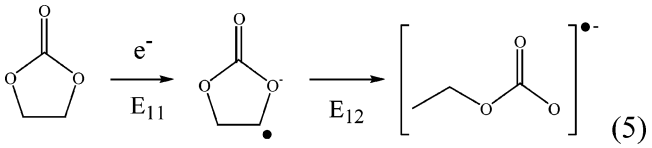


(5)

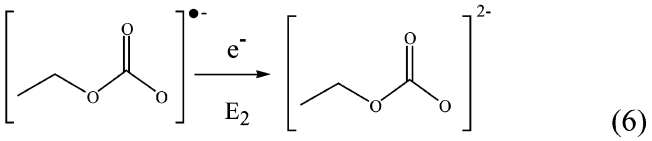


(6)

is involved; thus $E_1 = E_{11}$. The structures of the solvents and

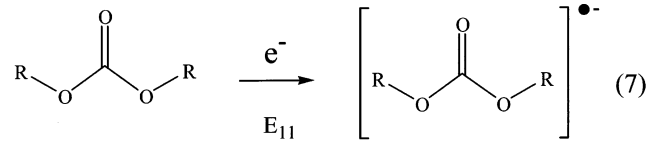


(7)

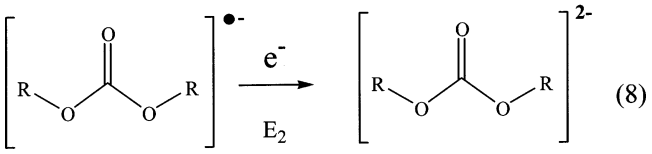


(8)

the additive examined here are illustrated in Figure 1. For the entropy and the thermal correction to the enthalpy, the frequency calculations were performed at the HF/6-31G(d) level, and the frequencies and the thermal corrections, both calculated at 298.15 K, and the zero-point energies were scaled by 0.8929.[70] The frequency calculations confirmed the true minima for the optimized structures.

Prior to the calculations for the molecules in question, electron affinities were computed at the same level of calculations (B3LYP/6-311+G(2d,p)//6-31G(d)) for a set of small molecules for which the experimental data are known. Figure 2 shows the correlation between the experimental and the calculated electron affinities of these molecules. The agreement is excellent with a standard deviation between the calculated and the experimental values[71] of 0.12 eV.

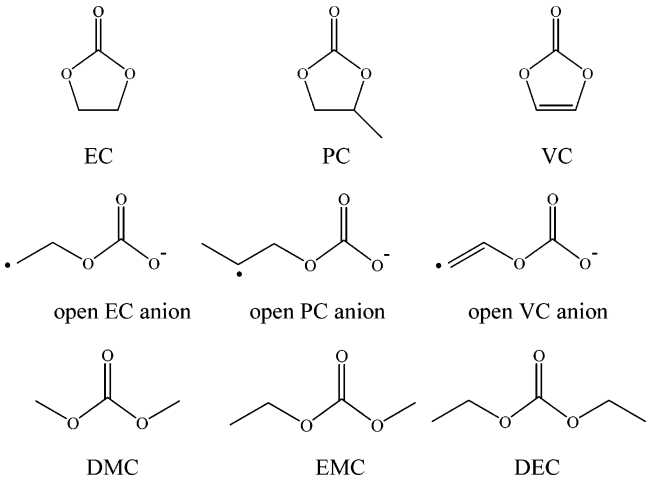


**Figure 1.** The solvents and the additive studied in this work. The locations of the double bond, the radical, and the negative charge in the open carbonate anions are only for presentation.

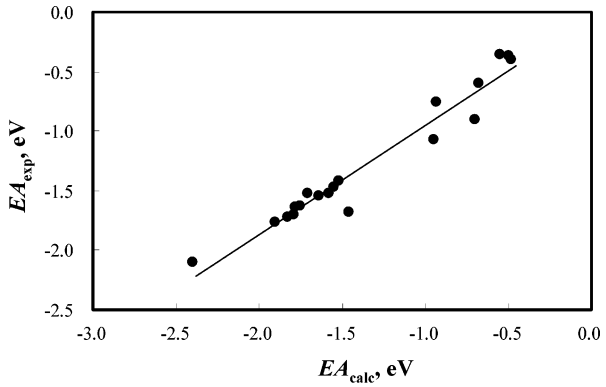


**Figure 2.** The experimental and the calculated electron affinities for a variety of small molecules. The level of calculations is B3LYP/6-311+G(2d,p)//6-31G(d). The standard of deviation is 0.12 eV. Here, EA is defined as EA = *G*(anion) − *G*(neutral), *G* being the free energy. The experimental values are taken from ref 71. The molecules include vinylidene, vinyl, acetaldehyde enolate, ethoxide, propargyl radical, acetone enolate, *n*-propyl oxide, isopropyl oxide, maleic anhydride, cyclobutanone enolate, 2,3-butanedione, butyraldehyde enolate, *tert*-butoxyl, cyclopentadienyl, pentadienyl, cyclopentanone enolate, 3-pentanone enolate, neopentoxyl, and cyclohexanone enolate.

The DFT calculations were also carried out in the solution. The solvent effect was included in both optimization and single-point calculations through the polarized continuum model using the polarizable conductor calculation model (CPCM).[72−76] The parameters used for the CPCM calculations are listed in Table 1. The dielectric constant for each solvent was taken from the literature,[77] while for VC it was weight-averaged to represent a 5 wt % solution in PC,[78] which is a typical application of VC in Li-ion battery electrolyte. For the open anions, the dielectric constant is that of the corresponding neutral solvent to model a single reduced open anion surrounded by the corresponding neutral solvent molecules. All ab initio and DFT calculations were performed, using Gaussian 98.[79]

In the discussion of the physical properties of solvent decomposition films, MD simulations have been performed to calculate bulk properties of the decomposition products: dilithium ethylene glycol dicarbonate (Li-EDC) and dilithium propylene glycol dicarbontate (Li-PDC), each being a major component in the decomposition of each solvent, EC and PC, respectively.[46] The structures of Li-EDC and Li-PDC are shown in Figure 3. The bulk properties such as the density and the cohesive energy were calculated from 500 ps MD simulations

**TABLE 1: Parameters Used for CPCM Calculations**

| | EC | | PC | | VC | | | | |
|---|---|---|---|---|---|---|---|---|---|
| | closed[a] | open[b] | closed[a] | open[b] | closed[a] | open[b] | DMC | EMC | DEC |
| $\epsilon$[c] | 89.78 | 89.78 | 66.14 | 66.14 | 72.16 | 72.16 | 3.08 | 2.98 | 2.82 |
| RSOLV[d] | 2.476 | 2.551 | 2.684 | 2.732 | 2.684 | 2.732 | 2.541 | 2.694 | 2.917 |

[a] A ring-closed structure. [b] A ring-open structure. [c] The dielectric constant, taken from ref 77. For VC, the value is weight-averaged to give 5 wt % of VC in PC with the dielectric constant of VC being 127. [d] The solvent radius in Å. The other parameters: the temperature (TABS), 298.15 K; the scaling factor (ALPHA), 1.2; the number of tesserae on each sphere (TSNUM), 60.

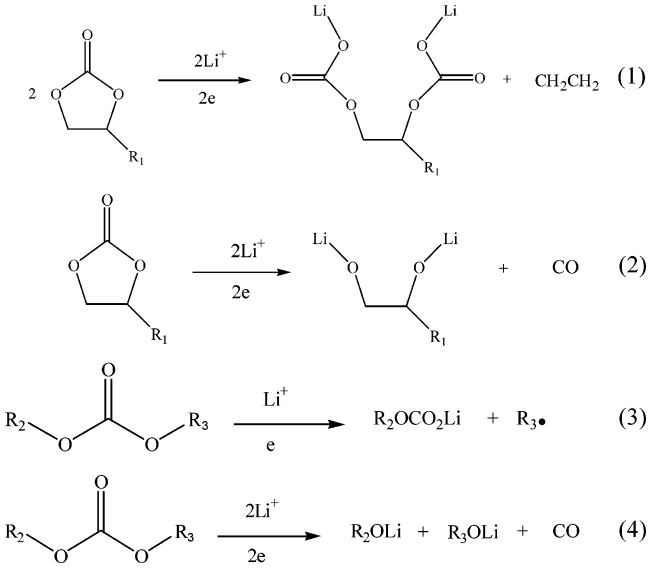


**Figure 3.** The decomposition reactions and the products for the solvents, for which the calculations were performed and the results presented in Table 4. In eqs (1) and (2), Li-EDC and Li-PDC are $R_1$ = H and $R_1$ = $CH_3$, respectively. In eqs (3) and (4), $R_2$ and $R_3$ are either $CH_3$ or $C_2H_5$. For example, when both $R_2$ and $R_3$ are $CH_3$, the reactions are for DMC.

of a box consisting of 40 molecules of each product under *NPT* conditions. The box was constructed by *Amorphous Builder* of Cerius[2] [80] and subject to 100 ps of equilibration before production runs. The cohesive energy may be calculated from the following equation:

$$E_{\text{cohesive}} = (\sum_{i}^{N} \sum_{i<j}^{N} E_{ij})/N \qquad (9)$$

where $E_{ij}$ is the intermolecular energy between molecules *i* and *j*, and *N* the number of molecules in the system. Equation 9 can be rewritten to eq 10:

$$E_{\text{cohesive}} = (E_{\text{tot}} - NE_{\text{gas}})/N = E_{\text{tot}}/N - E_{\text{gas}} \qquad (10)$$

where $E_{\text{tot}}$ is the total energy in the condensed phase, and $E_{\text{gas}}$ the energy for the single molecule in the gas phase. The values in eq 10 were averaged over the simulation.

The solubility property of the SEI film was obtained as an average from three independent runs of 500 ps MD simulations of a box of a decomposition product molecule in the solvent. The solvent was a reactant of the decomposition for the product, i.e., EC for Li-EDC and PC for Li-PDC. In the simulation, one product molecule (Li-EDC or Li-PDC) was immersed in a box of 100 well-equilibrated solvent molecules, and those solvent molecules which had van der Waals overlap with the decomposition product molecule were removed from the box, prior to the simulations. After removal of excess solvent molecules, the box was first subject to 500 steps of conjugate gradient minimization to relax the close contacts between molecules and subsequently 100 ps of equilibrium was run before production runs.

For MD simulations, all atoms were subject to integration of Newton's equation of motion with a time step of 1 fs. The force field was COMPASS,[81] which has been parametrized for condensed-phase simulations of mainly organic molecules. The electrostatic interactions were treated by the Ewald summation.[82] Bonds with hydrogens were constrained using the SHAKE algorithm.[83]

The interaction between the decomposition product and the graphite surface was characterized by *NPT* MD simulations of a box consisting of 6 layers of graphite sheets, each layer with 4 × 12 benzene rings, in one side of the box and 40 molecules of the dilithium alkylene glycol dicarbonates in the other side, having the decomposition product contacting the (1 0 0) plane of the graphite surface. The graphite structure was taken from the crystallographic data,[84] and the interface was constructed by Cerius[2]'s *Interface Builder*.[80] The temperature for all the MD simulations was set to be 300 K.

**TABLE 2: Electron Affinity of Cyclopentanone Enolate Predicted at Various Levels of Theory (eV)**

| level of theory | $\Delta E$[a] | $\Delta G$[b] |
|---|---|---|
| HF/6-31G(d)[c] | 0.445 | 0.460[d] |
| HF/6-31G(d,p)[c] | 0.445 | 0.460[d] |
| HF/6-311G(d)[c] | 0.249 | 0.264[d] |
| HF/6-31G(2d,p)[c] | 0.497 | 0.512[d] |
| HF/6-31+G(d,p)[c] | 0.027 | 0.042[d] |
| B3LYP/6-31+G(d,p)[c] | −1.462 | −1.44d[d] |
| B3LYP/6-311+G(2d,p)[c] | −1.512 | −1.497[d] |
| MP2/6-311+G(2d,p)[c] | −1.802 | −1.788[d] |
| B3PW91/6-311++G(2df,2p)[e] | −1.476 | −1.456[f] |
| expt[g] | | −1.596 |

[a] The electronic energy, $\Delta E = E$(anion) − $E$(neutral). [b] The Gibbs free energy, $\Delta G = G$(anion) − $G$(neutral). [c] The geometry was optimized at the HF/6-31G(d) level. [d] The frequency calculations and the thermal correction were performed at the HF/6-31G(d) level. [e] The geometry was optimized at the B3PW91/6-311++G(2df,2p) level.[f] The frequency calculations and the thermal correction were performed at the B3PW91/6-311++G(2df,2p)//B3PW91/6-311++G(2df,2p) level. [g] See ref 71.

## Results and Discussions

**Decomposition Reactions.** Theoretical calculations of Li battery electrolytes have been reported at various levels of accuracy.[25,50,62,63,85−90] Some of them were performed at HF levels,[25,85,86] and some at very high levels such as B3PW91/6-311+G(2df,2p).[63,87]

Here, we carried out a further validation of the theoretical model adopted in this work to reexamine the model chemistry for the reduction energy calculations. Well-established experimental data of electron affinity for the solvents studied here are scarce; thus, cyclopentanone enolate was chosen as a model compound for calibration. Table 2 lists the electron affinity for cyclopentanone enolate calculated at various levels of accuracy and compared with the experimental result obtained from

**TABLE 3: Thermodynamic Parameters for First-Electron and Second-Electron Reductions of Various Solvents and Additives in the Gas Phase and Solution (eV)[a]**

| | reaction | | EC | PC | DMC | EMC | DEC | VC |
|---|---|---|---|---|---|---|---|---|
| gas | 1st reduction | $\Delta E_{11}$ | 0.994 (0.347[b]) | 1.008 | | | | 0.652 (0.598[c]) |
| | | $\Delta H_{11}$ | 0.882 (0.330[b]) | 0.845 | | | | 0.460 (0.624[c]) |
| | | $\Delta S_{11} \times 10^3$ | 0.118 | 0.286 | | | | 0.040 |
| | | $\Delta G_{11}$ | 0.846 (0.308[b]) | 0.759 | | | | 0.448 (0.555[c]) |
| | | $\Delta E_1$ | −0.230 (−0.139[b]) | −0.152 (2.59[d]) | 1.306 (2.81[d]) | 1.211 | 1.284 | −0.050 (0.027[c]) |
| | | $\Delta H_1$ | −0.410 (−0.308[b]) | −0.269 | 1.188 | 1.103 | 1.175 | −0.176 (−0.113[c]) |
| | | $\Delta S_1 \times 10^3$ | 0.359 | 0.277 | 0.185 | 0.211 | 0.212 | 0.333 |
| | | $\Delta G_1$ | −0.518 (−0.455[b]) | −0.352 | 1.133 | 1.036 | 1.108 | −0.276 (−0.230[c]) |
| | 2nd reduction | $\Delta E_2$ | 3.230 (2.853[b]) | 3.120 | | | | 2.488 |
| | | $\Delta H_2$ | 3.193 (2.657[b]) | 3.068 | | | | 2.477 |
| | | $\Delta S_2 \times 10^3$ | −0.132 | −0.149 | | | | 0.024 |
| | | $\Delta G_2$ | 3.233 (3.013[b]) | 3.112 | | | | 2.484 |
| solution | 1st reduction | $\Delta E_{11}$ | −1.629 (−0.42[b]) | −1.523 | | | | −1.118 (−1.893[c]) |
| | | $\Delta H_{11}$ | −1.728 | −1.622 | | | | −1.311 (−1.925[c]) |
| | | $\Delta S_{11} \times 10^3$ | 0.104 | 0.068 | | | | 0.044 |
| | | $\Delta G_{11}$ | −1.760 | −1.642 | | | | −1.324 (−1.938[c]) |
| | | $\Delta E_1$ | −2.927 (−2.107[b]) | −2.919 | −1.415 | −0.465 | −0.399 | −2.495 (−2.440[c]) |
| | | $\Delta H_1$ | −3.102 | −3.064 | −1.524 | −0.572 | −0.506 | −2.625 (−2.492[c]) |
| | | $\Delta S_1 \times 10^3$ | 0.340 | 0.393 | 0.206 | 0.208 | 0.212 | 0.342 |
| | | $\Delta G_1$ | −3.203 | −3.181 | −1.586 | −0.634 | −0.569 | −2.727 (−2.605[c]) |
| | 2nd reduction | $\Delta E_2$ | −2.982 | −2.674 | | | | −3.81 |
| | | $\Delta H_2$ | −3.031 | −2.745 | | | | −3.694 |
| | | $\Delta S_2 \times 10^3$ | −0.111 | −0.224 | | | | 0.405 |
| | | $\Delta G_2$ | −2.997 | −2.678 | | | | −3.815 |

[a] Obtained from B3LYP/6-311+G(2d,p) calculations. The frequencies were calculated and the thermal corrections were made at the HF/6-31G(d) level of calculations for 298.15 K and were both scaled by 0.8929. The subscripts 1 and 2 refer to the first and the second reductions, respectively. $E_1 = E_{11} + E_{12}$. See eqs 1 and 2 in the text. [b] Taken from ref 63. [c] Taken from ref 87. [d] Taken from ref 25.

photoelectron spectroscopy.[71] The following points can be observed: (1) the results at the HF levels all have an opposite sign to those obtained by the post-HF calculations; (2) beyond the B3LYP/6-311+G(2d,p) level, little improvement is made in comparison to the experimental value, and the result by the optimization, the frequency calculations, and the single-point energy calculation at the B3PW91/6-311++G(2df,2p) level is even slightly worse than the value predicted by the B3LYP/6-311+G(2d,p)//6-31G(d) level. Though this calibration only does not immediately validate the latter level of theory for the solvents studied here, along with the calibration in Figure 2, it seems reasonable to use this model chemistry for reduction reactions of the solvents. We stress that it is not our aim here to determine the absolute values of electron affinities for the compounds of interest by calculation, but rather to examine the relative energetics of the reduction reactions for the solvents examined here.

In general, upon the first electron reduction, the carbonate group of the carbonate solvents undergoes a deformation from a flat structure for all the molecules examined, though still maintaining a quasi-cyclic structure except that the bond between the $O_{sp3}$ and $C_{sp3}$ atoms is now lengthened, consistent with the finding made by previous studies,[63,88] and then undergoes a spontaneous rearrangement to give a near flat plane in the open cyclic carbonate anions, as shown in eq 1. Furthermore, the bonds associated with the carbonate group tend to be stretched after reduction, more so for the second electron reduction, due to the increased antibonding nature after accepting two electrons, except for the $CH_{2(3)}-O$ bond upon the first electron reduction. As to the change in going from the gas phase to the solution, the largest changes arise from the carbonate group: most of the bonds further stretch. The change in the geometry tends to increase in a high dielectric constant medium, which is generally expected from the treatment used, i.e., the continuum model.

Table 3 lists the thermodynamic properties for the solvent reductions in both the gas phase and solution. It is immediately noticed that the gas phase reductions are all endothermic except for the ring-opening process, while the solution reductions are exothermic, for all the solvents and the additive in both one-electron and two-electron reactions. Whereas this is easily rationalized by the polarization effect in solution that stabilizes the reduction product with extra electrons, it is of interest to note the implication of the solvent effect on the solvent decomposition in the context of the SEI film formation. Endo et al. have reported that the solvent reductions of EC and PC were endothermic and became exothermic when coordinated with an $Li^+$ ion, based on Hartree−Fock ab initio calculations.[25] However, our calculations at a higher level clearly show that the solvent reduction can be exothermic without a $Li^+$ ion coordination in solution. Table 3 also includes the results from previous reports.[50,63,87,88] Though a comparison is not straightforward due to the lack of data and the different calculational procedures such as the way the solvent effect was taken into account, the results for the one-electron reduction of EC, PC, and VC in the gas phase are roughly consistent with those reported by Wang et al.[50,63,87,88] who performed even higher level calculations on the same compounds as the current study.

As far as the first electron reduction including the ring-opening process in solution is concerned, the order of the likelihood for the solvent reduction is EC > PC > VC > EMC > DMC > DEC, which is largely consistent with the finding by Zhang et al.[47,48] However, for the second electron reduction, VC has the lowest reduction free energy, lower than that of EC by as much as 1 eV, a substantial difference in the reduction potential. Thus, VC is more likely to undergo the two-electron decomposition to give products such as $Li_2CO_3$ (see eq 1), a stable SEI film component, or to produce lithium alkoxides (see eq 1 in Figure 3). Polymerization of one-electron reduction products of VC on the graphite surface has been recently suggested[51] and may occur in parallel to the two-electron decomposition, though a low concentration of VC, ∼5 wt %, is unlikely to make the polymerization of VC a dominant process.

**TABLE 4: Thermodynamic Properties for Decomposition Reactions of Various Solvents (eV)[a]**

| | EC | | PC | | DMC | | EMC | | DEC | |
|---|---|---|---|---|---|---|---|---|---|---|
| eq[b] | 1 | 2 | 1 | 2 | 3 | 4 | 3 | 4 | 3 | 4 |
| $\Delta E$ | −18.724 | −13.939 | −18.634 | −13.894 | −7.01 | −13.534 | −7.003[c]/−7.004[d] | −13.551 | −7.000 | −13.571 |
| $\Delta H$ | −19.442 | −14.52 | −18.957 | −14.219 | −7.3097 | −13.992 | −7.302[c]/−7.272[d] | −14.003 | −14.700 | −21.451 |
| $\Delta S$ | −0.0042 | −0.0017 | −0.0439 | −0.0216 | 0.00029 | 0.00027 | 0.00030[c]/0.00038[d] | 0.00028 | −0.023 | −0.023 |
| $\Delta G$ | −18.197 | −13.996 | −18.193 | −13.948 | −7.3978 | −14.073 | −7.391[c]/−7.385[d] | −14.086 | −7.758 | −14.480 |

[a] Calculated by B3LYP/6-311+G(2d,p) calculations. See the footnote in Table 3 for $\Delta E$, $\Delta H$, $\Delta S$, and $\Delta G$. [b] See Figure 3. [c] When a methyl radical is one of the products. [d] When an ethyl radical is one of the products.

We have also attempted calculations for the reduction potentials of the solvents in the presence of a lithium cation which formed a complex with the carbonyl oxygen of the solvent molecules. The first reduction free energies were −5.25, −5.05, and −4.77 eV for lithiated EC, PC, and VC, respectively. Similar results have been reported.[63,87] While the reduction energies are more exothermic in the presence of a positive lithium ion, the order in the likelihood of reduction among the solvents remains the same. As to the second reduction reaction, optimization failed to locate the two-electron anions except for all but a few solvents.

Balbuena and co-workers have examined the role of VC in the PC electrolyte and found that VC stabilizes the reduction ion-pair intermediate of PC, thus promoting reduction of PC to form SEI film materials,[50] and further suggested that the VC reduction product is more compact and has more favorable interactions with the graphite surface, compared to either EC or PC decomposition products.[91,92] Yet, their calculations on the interactions with the graphite were based on a single solvent molecule on the surface of graphite, ignoring intermolecular interactions among solvents,[91] and the calculations on the association energies only dealt with up to tetramers of the decomposed molecule in the gas phase.[92] As to the difference between EC and PC, they claimed that the stronger affinity of a Li ion to PC than to EC causes a preferred co-intercalation of the solvent to graphite, thus leading to exfoliation of graphite. However, the predicted difference in the enthalpy of Li coordination to the solvent between the PC···Li complex and the EC···Li complex was only 1.5 kcal mol$^{-1}$. With this small energy difference, a considerable amount of the EC···Li complex can co-intercalate as well. More realistically, it has been suggested that the intercalation of solvated Li ions into graphite follows a step in which the Li ions lose their solvated molecules ($m$) from the original number of solvated molecules ($n$) for faster co-intercalation, as follows.[35]

$$\mathrm{Li(sol)}_n \rightarrow \mathrm{Li(sol)}_{n-m} + m(\mathrm{solv}) \qquad (11)$$

Hence, stable Li ions solvated by the solvent molecules with a higher affinity to Li ions disfavor this process and thus may have less tendency for co-intercalation, contrary to the authors' claim.[50] Their study also found that the reactivity and the solvent decomposition mechanism are very similar between EC and PC. Recently, Ogumi and co-workers have found particle-like precipitates on the graphite surface in the PC electrolyte in the presence of VC, which seemed to have prevented co-intercalation of PC.[31] The precipitates may be the polymer composed of the first electron reduction product of VC or the second electron reduction product.

We also tested the behavior of the second electron reduction for trifluoropropylene carbonate (TFPC), another well-known electrolyte additive.[93] The calculated second electron reduction free energy for TFPC was −3.768 eV, again much lower than that of EC or PC. Thus, the very low second electron reduction energies of VC or TFPC could play a role in the decomposition of these additives at the anode−electrolyte interface and may provide insight into their proven effectiveness as additives. Yet, at this point, the most likely second electron reduction decomposition mechanism of VC or TFPC is unclear and also no direct evidence of the second electron reduction product has been found, though CO gas has been detected as indirect evidence for the formation of alkoxide from VC in the following reaction: VC + 2e → $^{-}$OCH═CHO$^{-}$ + CO.[52] A further study on the nature of the VC decomposition is warranted.

For the linear carbonates, it was difficult to reach convergence during the geometry optimization in the second electron reduction step, possibly a sign of instability. It is probable that upon the second electron transfer, the molecule is decomposed immediately to give reduction products.

As has been pointed out by other researchers,[47,48,50,63] the difference in the calculated reduction characteristics between EC and PC is not significant, which provides little explanation for the sharp contrast between them during the recharging cycle of a Li-ion battery. Likewise, the difference in the reactivity among the linear carbonates, DMC, EMC, and DEC, is also unsubstantial.

Additionally, we have performed free energy calculations on the decomposition reactions proposed by the recent in situ gas analysis experiments[46] which are illustrated by Figure 3. Table 4 lists the results for the decomposition reactions shown in Figure 3. Our calculations indicate that for EC and PC, eq 1 in Figure 3 is thermodynamically preferred, while eq 4 is more likely for the linear carbonates. Indeed, alkyl dilithium carbonates (eq 1 in Figure 3) from EC and PC and lithium alkoxides (eq 4 in Figure 3) for the linear carbonates have been found to be the dominant products according to the in situ analysis of the gas products.[46] Still, the calculations on reactivity failed to explain the difference among solvents in their cycle behaviors. Next, we will examine the physical properties of solvent decomposition products.

**Dilithium Alkylene Glycol Dicarbonate Film Bulk Properties.** Aurbach et al. have proposed a model to explain the difference in the behavior of Li intercalation between the EC- and PC-based electrolytes in terms of the cohesiveness of the passivation films.[64] The model suggested that the reduction products of EC form a very cohesive film quickly before solvent co-intercalation which otherwise leads to graphite exfoliation, while the PC decomposition products lack cohesiveness and also film formation is slow, allowing the co-intercalation to proceed. They attributed the difference in the behavior of SEI film formation to the methyl group of PC which may prevent a buildup of cohesive film. Here, we first examined the bulk properties of the main products from the solvent decompositions of the EC-based and PC-based electrolytes and then also the interactions of the products with the graphite surface.

Before the analysis of the solvent decomposition products, we tested the performance of the current modeling protocol including the force field adopted in this work in predicting the densities and the heats of vaporization for the solvents used,

**TABLE 5: Averaged Properties of Solvents Predicted from MD Simulations[a]**

| properties | EC | PC | DMC | EMC | DEC |
|---|---|---|---|---|---|
| temperature, K | 309.51 ± 10.2[b] | 293.59 ± 10.77 | 294.59 ± 12.01 | 297.6 ± 11.9 | 294.2 ± 8.0 |
| cubic box size, Å | 16.97 ± 4.91 | 18.02 ± 4.07 | 14.28 ± 4.68 | 26.82 ± 3.43 | 27.96 ± 3.02 |
| density, g cm$^{-3}$ | 1.24 ± 0.03 (1.322)[c] | 1.16 ± 0.03 (1.198)[c] | 1.03 ± 0.04 (1.071)[c] | 1.03 ± 0.02 (1.007)[c] | 0.99 ± 0.02 (0.98)[c] |
| heat of vaporization, kcal mol$^{-3}$ | 14.5 ± 1.7 (15.68)[d] | 14.3 ± 1.7 (15.56)[d] | 8.2 ± 1.9 (9.26 ± 0.06)[e] | 9.7 ± 1.8 (10.27 ± 0.95)[e] | 10.4 ± 1.6 (10.41 ± 0.04)[e] |

[a] The values were averaged over 500 ps of simulations. [b] The melting point of EC is 310 K. [c] The experimental data at 298 K (see refs 77 and 94). [d] The experimental data extrapolated to 298 K (see ref 95). [e] The experimental data measured at 298 K (see refs 96−98).

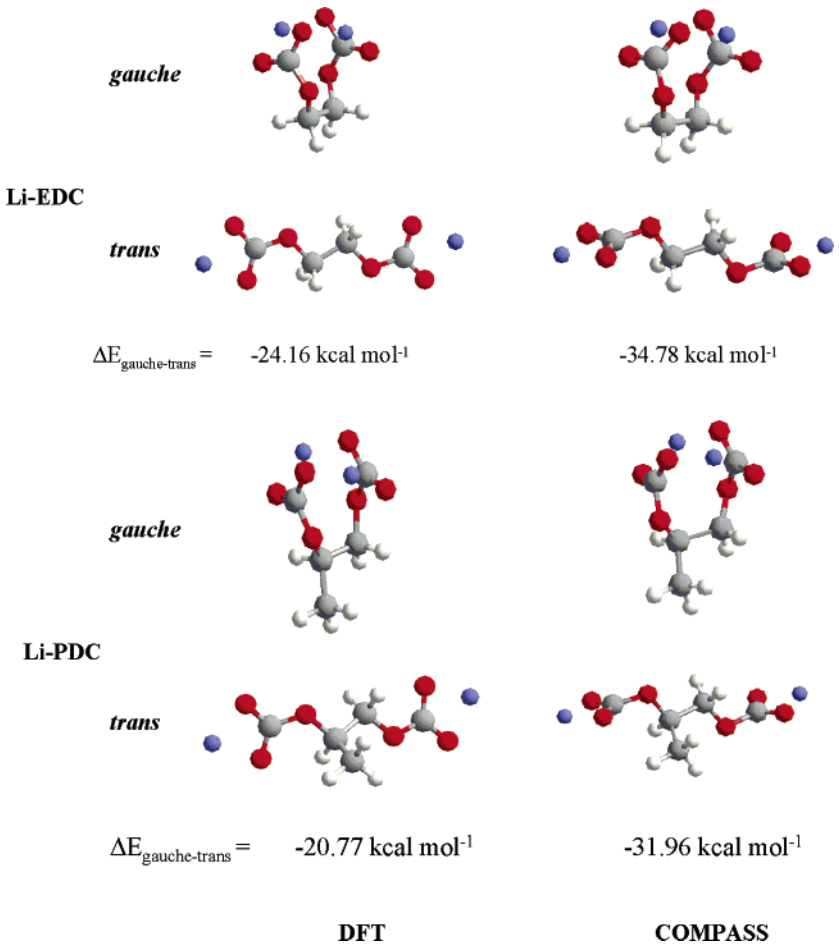


**Figure 4.** The optimized structures and the energies of Li-EDC and Li-PDC in the gauche and trans forms, predicted by HF/6-31G(d) and B3LYP/6-311+G(2d,p), respectively. $\Delta E_{\text{gauche-trans}} = E(\text{gauche}) - E(\text{trans})$. The results are compared to those obtained by force field minimization using COMPASS.

which are summarized in Table 5. The *NPT* simulations were run for a box of 50 solvent molecules, and the calculated properties were averaged over 500 ps of simulations after equilibration. A comparison with the experimental data is favorable.[77,94−98]

Since the conformation of the decomposition compounds affects the physical properties, their conformational stability was also examined. Both B3LYP/6-311+G(2d,p)//6-31G(d) calculations and force field minimizations predicted that both Li-EDC and Li-PDC prefer the gauche conformation around the central C−C bond, in which the two positively charged lithium cations are shared by the two negatively charged carbonate groups rather than being half exposed in the trans form (see Figure 4), as shown in Figure 4. Though COMPASS overestimates the gauche energy over trans somewhat for both compounds, the conformational preference is well reproduced by the force field. Structurally, both DFT and COMPASS optimized complexes are very similar, except that the COMPASS force field predicts the carbonate group in trans twisted around the $C_{sp2}-O_{sp3}$ bond by 90° from that predicted by the DFT calculations. This difference is not expected to affect the bulk properties significantly.

As the starting configuration for the bulk simulations, the lithium ions of the alkylene glycol dicarbonates were initially located at 1.63 Å from each one of the carbonate oxygen atoms of the terminal carbonate groups, for both Li-EDC and Li-PDC, with the carbonate oxygens surrounding the lithium ions, shown as gauche in Figure 4, obtained from force field minimization in the gas phase, and no constraint was used. During the simulation, some of the lithium ions moved away from the vicinity of the original carbonate oxygens which resulted typically, but not always, in a conformational transition of the alkylene glycol dicarbonate from gauche to trans around the central C−C bond due to the interactions with neighboring molecules, during the simulation. The averaged gauche fraction

**TABLE 6: Bulk Properties and Solubility of the Decomposition Products from EC and PC**

Bulk Properties

| | temperature, K | volume, Å$^3$ | density, g cm$^{-3}$ | cohesive energy, kcal mol$^{-1}$ |
|---|---|---|---|---|
| Li-EDC | 296.88 | 2886.75 | 1.86 | −67.28 |
| Li-PDC | 293.71 | 4682.09 | 1.41 | −64.47 |

Heat of Dissolution for the Decomposition Compounds (kcal mol$^{-1}$)

| | solvent | $\Delta H_{sub}$ | $\Delta H_{sol}$ | $\Delta H_{diss}$ |
|---|---|---|---|---|
| Li-EDC | EC | 67.28 | −46.62 | 20.66 |
| Li-PDC | PC | 64.47 | −107.04 | −42.57 |

for Li-EDC was around 0.8 and that for Li-PDC was somewhat smaller, considerably less than those in the gas phase.

Table 6 lists the bulk properties of Li-EDC and Li-PDC, demonstrating a clear difference between the two decomposition products in that Li-EDC has a higher density and more cohesive energy than Li-PDC. This suggests that the EC-based SEI film is denser and less brittle, a favorable characteristic for an SEI film, than the PC counterpart. Similar discussions have been made for the difference between the EC- and PC-based films.[92] Close inspection of the MD trajectories revealed that the difference between the two films stems from the methyl group of Li-PDC that prevents molecules from packing themselves close to one another. The difference in cohesive energy between Li-EDC and Li-PDC is line with the previous report on binding energies for trimers of the same products by high-level DFT calculations.[92]

For the quantitative discussion on the structural difference between the two decomposition products, the pair distribution function is shown in Figure 5 for the central carbon atoms ($CH_2$ or CH), $g_{Csp3-Csp3}$, for the glycol dicarbonates. The distribution function excludes the intramolecular contribution. From the figure, the average next-neighbor intermolecular distance, measured as the distance between the central carbon atoms belonging to the next-neighbor dicarbonates, is 3.9 Å for Li-EDC, whereas that for Li-PDC is 4.2 Å. Further, the integration of the distribution function shows that there are more next-neighboring molecules around Li-EDC than around Li-PDC. The average Li···$O_{sp2}$ distance was 1.7 Å. The larger area in the first peak for Li-EDC than for Li-PDC is primarily due to the absence of the methyl group in Li-EDC which otherwise pushes each molecule apart from one another, which is the case for Li-PDC. Figure 6 presents representative snapshots illustrating the association of Li-EDC and Li-PDC from the simulations. The central Li-EDC molecule is associated with four other molecules at one end of the molecule and with three at the other end through Li coordination, while Li-PDC has three other

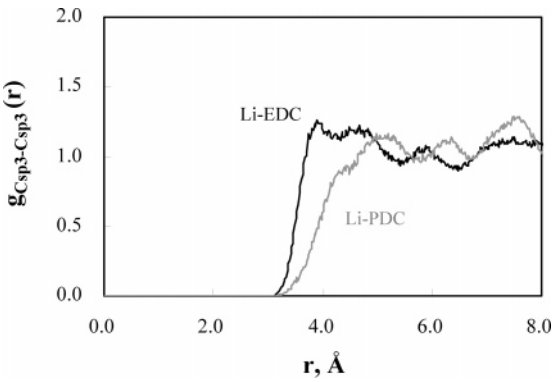


**Figure 5.** The pair distribution function for the $C_{sp3}-C_{sp3}$ pair for Li-EDC and Li-PDC. The $C_{sp3}$ atom refers to the central carbon atom of the alkylene glycol dicarbonates.

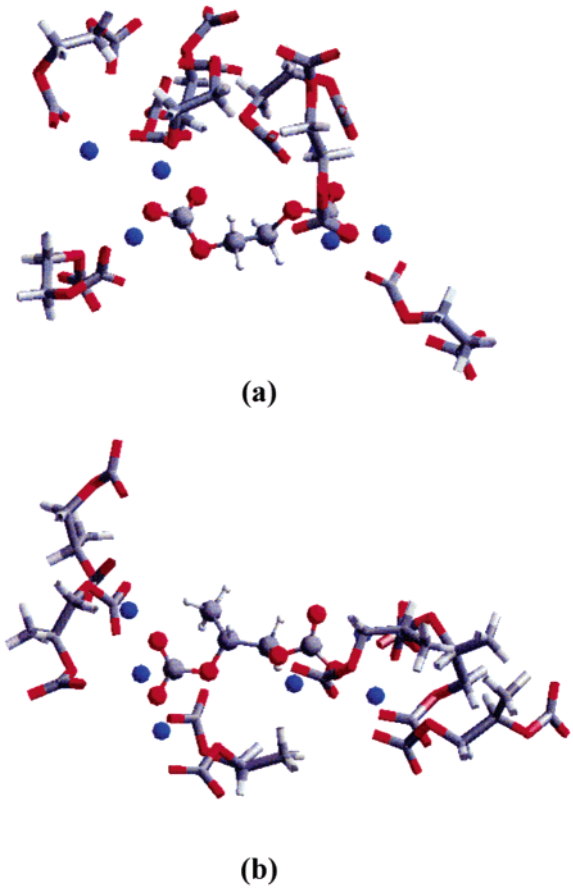


**Figure 6.** Snapshots from MD simulations of (a) Li-EDC and (b) Li-PDC. Only a molecule, represented by a ball-and-stick model, with immediate neighbors, by a cylinder model, is presented to show the molecular association. The central Li-EDC molecule is associated with four other molecules at one end of the molecule and with three at the other end through Li coordination, while Li-PDC has three other molecules at both ends.

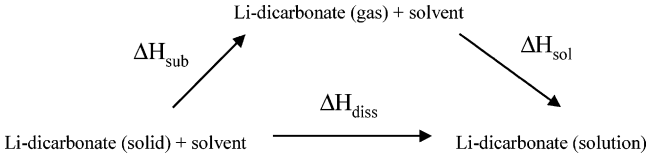


**Figure 7.** The thermodynamic cycle for the dissolution of dilithium alkylene glycol dicarbonate into the solvent.

molecules at both ends. It was observed that the alkylene glycol dicarbonate molecules are connected to one another in an extensive network through Li ion coordination, which is the main reason for the high cohesive energies for both products.

The solubility of the decomposition products into solvent was also examined. With the thermodynamic cycle illustrated in Figure 7, the heat of dissolution was calculated by the following equation:

$$\Delta H_{diss} = \Delta H_{sub} + \Delta H_{sol} \quad (12)$$

where $\Delta H_{sol}$ and $\Delta H_{sub}$ are the heat of solution to the solvent and the heat of sublimation for the film, respectively, as follows:

$$\Delta H_{sub} = \Delta E_{sub} + P\Delta V - RT \quad (13)$$

$$\Delta H_{sol} = \Delta E_{sol} + P\Delta V - RT \quad (14)$$

where $\Delta E_{sub}$ is the sublimation energy of the decomposition

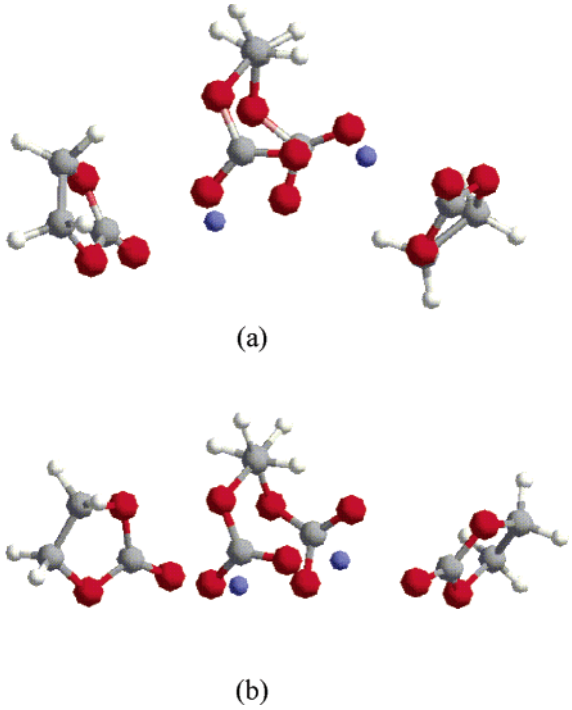


**Figure 8.** The solvation structures of Li-EDC optimized by (a) HF/6-31G(d) calculations and (b) force field minimizations.

product, the energy required to bring the decomposition molecule from the condensed state to the ideal gas phase, and $\Delta E_{sol}$ is the energy require to transfer the decomposition molecule from the ideal gas phase to the solution. For Li-ECD as an example of the decomposition molecule,

$$\Delta E_{sol}^{Li\text{-}EDC} = E_{sol}^{Li\text{-}EDC} - E_{sol}^{EC} - E_{gas}^{Li\text{-}EDC} \quad (15)$$

where $E_{sol}^{Li\text{-}EDC}$, $E_{sol}^{EC}$, and $E_{gas}^{Li\text{-}EDC}$ are the energy of the Li-EDC solution (a single Li-EDC molecule in the EC solvent), the EC bulk solvent, and a single Li-EDC molecule in the gas phase, respectively. $P$, $V$, $R$, and $T$ are the pressure, the volume, the gas constant, and the absolute temperature, respectively. The simulations were performed under zero pressure; thus the $P\Delta V$ term disappears in eqs 13 and 14.

In predicting a heat of solution, the interaction between the solute and the solvent is the key factor determining the quality of the prediction. To examine how well the interaction is described by the current force field, a comparison with DFT calculations was made. First, a simulation of a box having 1 Li-EDC in 50 EC molecules was run for 200 ps after equilibration, to model the solvation of Li-EDC by EC. The first solvation shell of Li-EDC was monitored from one frame to the other at different points of the simulations: at 50, 100, and 200 ps. In particular, the number of solvent molecules in the first shell, their geometrical orientation with respect to the solute, and the distances between the solvent molecules and the solute were compared. The first solvation shell had one Li-EDC molecule surrounded by eight EC molecules, and the shell structure changed somewhat in going from 50 to 100 ps but differed little between the structures at 100 and 200 ps; thus, the one at 200 ps was chosen as the representative solvation structure. To be computationally affordable, of the eight EC molecules, only two coordinated directly with the Li ions of Li-EDC were considered for further examination and used as the initial structure for optimization at the HF/6-31G(d) level, followed by B3LYP/6-311+G(2d,p) single-point calculations to estimate the semisolvation energy. The optimized structures are shown in Figure 8. Then, the semisolvation energy ($\Delta E_{Li-EDC-EC}$) was estimated by subtracting the energy before and after the solvation:

$$\Delta E_{Li-EDC-EC} = E_{Li-EDC-EC} - E_{Li-EDC} - 2E_{EC} \quad (16)$$

where $E_{Li-EDC-EC}$, $E_{Li-EDC}$, and $E_{EC}$ are the electronic energy of the semisolvation structure, a single Li-EDC molecule, and a single EC molecule all in the gas phase, respectively. The basis set superposition error was ignored in the calculations. The interaction energy was also calculated by force field minimization in which the steepest decent was first used, followed by the adopted Newton−Raphson method and the quasi-Newton method. The solvation energy calculated by the force field minimization was −29.57 kcal mol$^{-1}$, very close to the result from the DFT calculations, −27.81 kcal mol$^{-1}$. As is shown in Figure 8, though a slight difference appears in the orientations of the solvent molecules with respect to the solute, the overall solvation structures are similar between the two calculations.

Table 6 also lists the heat of solution ($\Delta H_{sol}$), the heat of sublimation ($\Delta H_{sub}$), and the heat of dissolution ($\Delta H_{diss}$) for the two decomposition products Li-EDC and Li-PDC in the EC and PC solutions, respectively. The results indicate a sharp contrast in that Li-PDC is soluble in the solvent, while Li-EDC is insoluble, due to the higher heat of solution for Li-PDC than Li-EDC. The main conclusion that can be drawn from the simulations is that Li-PDC is more soluble in PC than Li-EDC in EC.

The above difference in the heat of solution between the two dilithium alkylene glycol dicarbonates is mainly caused by the larger intermolecular space, or free volume, in the PC solvent, 140 Å$^3$ molecule$^{-1}$, almost twice that in the EC solvent, 79 Å$^3$ molecule$^{-1}$. The free volumes were calculated by subtracting the total molecular volume in a simulation box from the box volume and then divided by the total number of molecules, obtained from the above MD simulations of the solvents. Thus, the PC solvent with a greater space between molecules, created primarily by the methyl group, can better accommodate a large molecule such as Li-PDC into the system. Entropically, the less symmetric and more bulky PC molecule, coupled by the greater intermolecular space for rearrangement of the PC solvent molecules around the solute, may help promote the dissolution of Li-PDC as well, compared to Li-EDC in the EC solution. Yet, while the predicted difference in the bulk properties and the solubility between the EC- and PC-based decomposition compounds is of relevant interest, the difference should not be too emphasized. It should be recalled that a PC-based electrolyte does allow recharging in the presence of VC, suggesting that a PC-based SEI film does hold on the graphite surface with the help of VC. Still, the dissimilarities in the film quality between the EC-based and PC-based decomposition compounds are likely to cause the contrasts in battery performance such as cycle life.

**Interactions of Dilithium Alkylene Glycol Dicarbonate Film with the Graphite Surface.** Once the solvent decomposition occurs, the products should have a reasonable adhesive property to the graphite surface for further buildup of SEI film and the life stability of the film. Here, we examine the interactions of the decomposition products with the graphite surface. First, the interaction of an individual decomposition compound with the graphite was evaluated. This was to understand the basic interaction between the decomposition compound and the graphite surface without the possible effect which graphite may have on the structure of the decomposition molecules near the interface which may be different from that in the bulk.

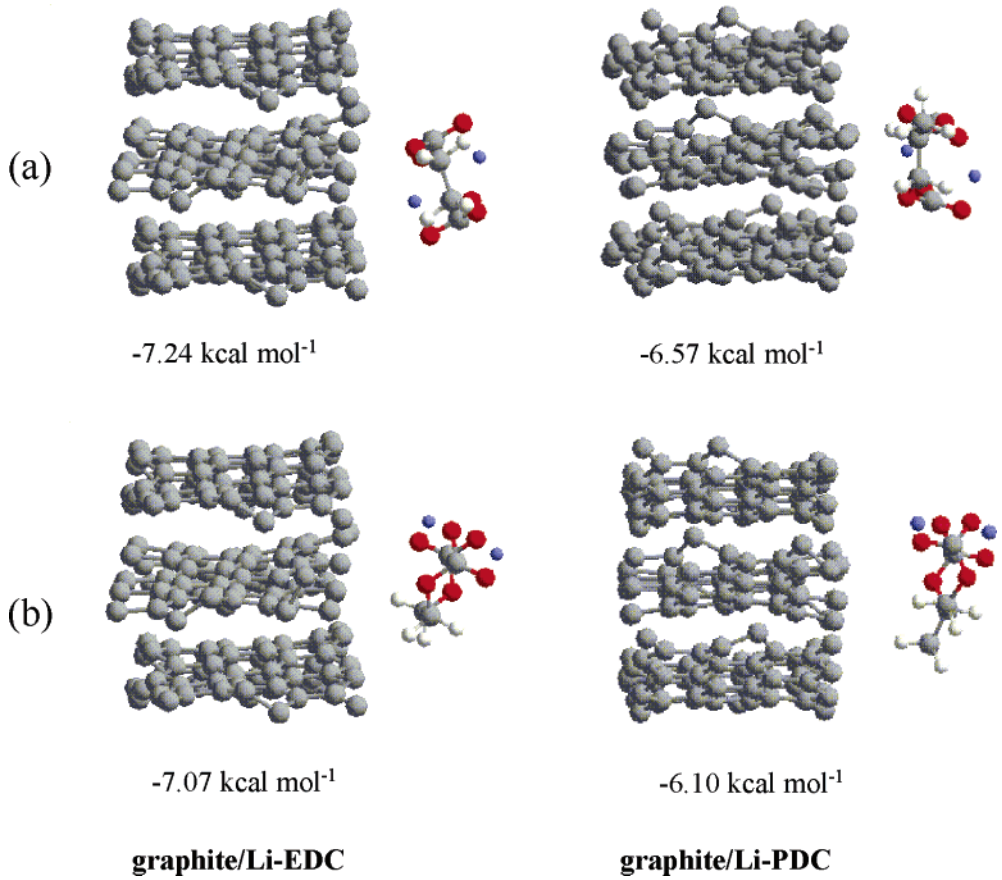


**Figure 9.** Minimum energy structures for Li-EDC and Li-PDC near graphite obtained from quenched dynamics simulations: (a) one with the central C−C bond parallel to the graphite sheets and (b) the other perpendicular. The graphite sheets are viewed so that they are perpendicular to the figure plane. Only three layers of graphite are shown for clarity. The energies shown are the adhesive energies.

Lithium ion intercalation occurs at the edge site rather than the basal plane of graphite. On the other hand, Peled and co-workers have suggested that organic components of SEI film reside on the basal plane rather than at the edge site.[99] However, their conclusion was largely based on the elemental analysis of the SEI film components, thus inconclusive, and furthermore, our own data confirmed some organic components on the edge site as well.[52] Here, we placed the decomposition product molecule near the (1 0 0) plane of graphite sheets which had five layers of graphite sheets, each layer with 24 benzene rings, which were constructed from the crystallographic data.[84] Then, quench dynamics was run at 1000 K for 10 000 steps during which the structure was subject to 500 steps of minimization at every 500 steps of dynamics simulation. The global minimum structure was found by searching for the lowest energy structure with the energy $E_{min}$ (product|graphite) from the quench dynamics simulation. Once the global minimum structure was found, the breakdown of the energy contribution, one from the graphite ($E_{min}$(graphite)) and the other from the decomposition molecule ($E_{min}$(product)), was performed independently to extract the adhesive energy:

$$\Delta E_{ad} = E_{min}(\text{product|graphite}) - E_{min}(\text{product}) - E_{min}(\text{graphite}) \quad (17)$$

It was found that there were basically two global minima for each product, Li-EDC and Li-PDC, the orientations of which are shown in Figure 9, along with the adhesion energies, with respect to the graphite surface: (a) one with the central C−C bond of the decomposition molecule perpendicular to the graphite sheets and (b) the other parallel to the graphite. For Li-EDC, each orientation, orientation a or orientation b, has its energetic equivalent which is obtained by rotating around the $C_2$ axis of the molecule, not shown in the figure. On the other hand, Li-PDC has no such equivalent due to its lower degree of molecular symmetry. Figure 9 also indicates that the adsorption energy of Li-EDC to graphite is somewhat higher than that of Li-PDC.

Though a breakdown of the adhesion energy into contributions from each group of the molecule was not performed, it is suspected that the methyl group of Li-PDC somehow hinders the adhesion to the graphite. This can be well illustrated by the difference between Li-EDC and Li-PDC in orientation b with respect to the graphite surface in Figure 9. The preferable interaction between the methyl group and the graphite pushes the center of gravity of Li-PDC away from the graphite, thus resulting in a smaller overall interaction with the graphite than Li-EDC. Additionally, it is also important to point out that while each Li-EDC orientation has an energetically equivalent structure, Li-PDC has no such equivalent but has two more orientations similar to orientations a and b by rotation around the axis perpendicular to the C−C bond in orientations a and b, having smaller adsorption energies by approximately 0.8 kcal $mol^{-1}$ than those for orientations a and b in Figure 9, respectively. It follows that Li-PDC has to undergo reorientation of the molecule on the graphite surface in order to have a favorable interaction with graphite during the SEI film formation process and thus, it takes longer than Li-EDC which has a higher degree of symmetry. The slower buildup of an SEI film in a PC-based electrolyte has been suggested by Aurbach et al.[64]

Next, to examine the interactions between the graphite surface and the decomposition product as a condensed material, an

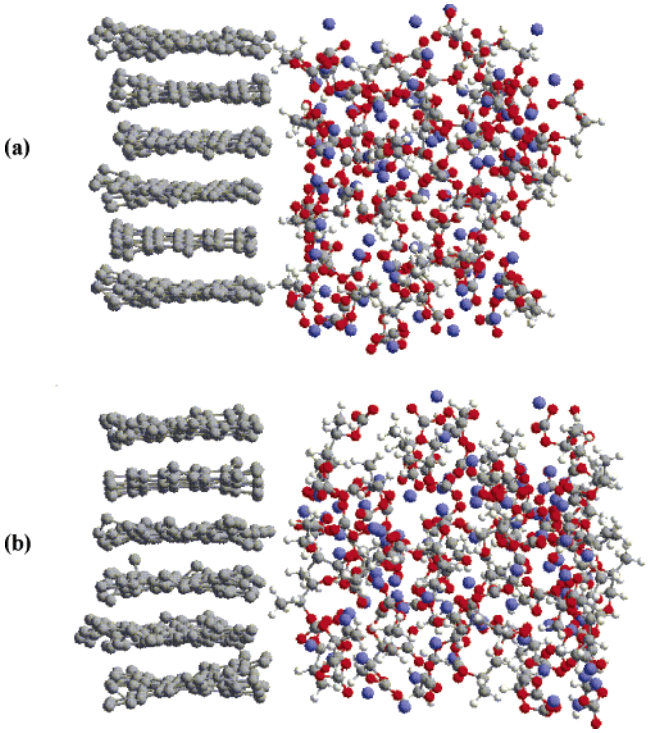


**Figure 10.** Snapshots of (a) the Li-EDC/graphite and (b) the Li-PDC/graphite interface taken from the MD simulations.

interface between them was constructed, using the same graphite sheets as above. For the interface, the box of Li-EDC (or Li-PDC) was taken from the last step of the simulation for the above bulk property calculations which was combined with the graphite sheets through *Interface Builder*[80] to create an interface between the graphite and the decomposition product, having 4 Å for the interface gap between the two systems. The interface was created so that the electrolyte faces the (1 0 0) plane of graphite.

One-nanosecond *NPT* simulations were run for each interface after equilibration, and the calculated density averaged over the simulation was 1.56 g $cm^{-3}$ for Li-EDC|graphite and 1.35 g $cm^{-3}$ for Li-PDC|graphite. The averaged total potential energy was subtracted by the potential energy of the graphite sheets obtained from a separate 500 ps *NPT* simulation of the graphite sheets alone and also the potential energy of the bulk Li-EDC or Li-PDC obtained from the bulk simulations above. The resultant interaction energy between the dicarbonate and graphite was −0.45 and −0.38 kcal $mol^{-1}$ $Å^{-2}$ for Li-EDC|graphite and Li-PDC|graphite, respectively. The energies were divided by the graphite surface area facing the decomposition molecules. As is expected from the adhesive energy of the individual molecule to the graphite surface, Li-EDC seems to have a more favorable interaction with graphite than Li-PDC as a film as well. Repeated independent simulations also indicated the same trend, showing the statistical legitimacy of the result.

To further understand the nature of the film components near the graphite, we analyzed the interface structure of each decomposition compound. Figure 10 depicts snapshots of the interface for both systems obtained from the simulations. At a glance, the Li-EDC molecules seem more packed and also close to the graphite surface, while the Li-PDC molecules are less dense and show some disorder at the interface. To examine how far the solute molecules were from the edge of the graphite sheets in more detail, the pair distribution functions were calculated from the simulation trajectories between each atom of the Li-EDC or the Li-PDC molecules and the carbon atoms

**TABLE 7: Averaged Number of Atoms of Li-EDC/Li-PDC near the Graphite Obtained from the Pair Distribution Functions**[a]

| | $N$[=O][b] | $N$[−O−][c] | $N$[$CH_2$][d] | $N$[$CH_3$][e] | $N$[=C][f] | $N$[Li][g] |
|---|---|---|---|---|---|---|
| Li-EDC | 0.56 | 1.99 | 2.35 | | 0.74 | 0.37 |
| Li-PDC | 0.13 | 0.26 | 0.43 | 1.08 | 0.11 | 0.07 |

[a] The number was obtained from integration of the pair distribution function for the atom in question and the carbon atoms at the graphite edge out to 4 Å. [b] The number of carbonyl oxygen atoms including the charged oxygen atoms. [c] The number of ester oxygen atoms. [d] The number of methylene atoms. [e] The number of methyl atoms. [f] The number of carbonyl carbon atoms. [g] The number of lithium ions.

at the edge of the (1 0 0) plane facing the decomposition product. Table 7 indicates the averaged number of atoms of the decomposition molecule within 4 Å from the carbons at the edge of the graphite (1 0 0) surface, obtained from integration of the pair distribution functions out to 4 Å. From the table, a picture can be drawn that both decomposition compounds orient themselves with respect to the graphite surface with the methyl/methylene group leaning toward the graphite and the carbonate groups away from it. As to the difference between the two decomposition compounds, clearly the Li-EDC molecules interact more closely with the graphite, implying a better adhesion to the graphite than the Li-PDC molecules. The methyl group of a Li-PDC molecule points itself toward the graphite, pushing the rest of the molecule away from the graphite surface. Here, again, the methyl group plays a chief role in the difference between the two decomposition products interacting with graphite. Balbuena and Wang have reported adsorption energies of the reduction products of VC, EC, and PC on a graphite surface.[88] However, the calculations were performed for the interactions between a single molecule of the product and the basal plane of graphite by a high-level DFT method; thus the comparison with the current study is not straightforward. Still, their study shows that the distance between Li-EDC and graphite is closer than that between Li-PDC and graphite, which is in line with our results.

The effect of the graphite interface on the structure of the nearby decomposition compound was inspected as well through the pair distribution functions from the interface simulations and compared to those obtained from the bulk simulations. The molecules included in the pair distribution functions were those within 15 Å from the graphite (1 0 0) surface. Mostly, the differences in the structures between the bulk and the interface are similar for both decomposition compounds, seemingly showing a comparable degree of effect by the graphite on the nearby structure for both Li-EDC and Li-PDC. Yet, the largest effect of the graphite appears on the structures associated with the methyl carbon of Li-PDC, as is shown in Figure 11, especially for the $CH_3-CH_3$ and the $CH_3-O(=C)$ interactions.

These results seem to suggest that Li-PDC has a more altered structure near the graphite surface than Li-EDC, possibly caused by the preferable interaction between the methyl group and the graphite surface, though the observation on the methyl group interactions alone does not provide enough support for the claim. Still, it is possible that the structural difference between the bulk and the interface for Li-PDC, associated with the methyl group, also accounts for the difference in the interaction energy between the Li-EDC|graphite and Li-PDC|graphite systems. Further analysis of the interaction between the decomposition compound and the graphite is needed. Also, the force field COMPASS may not be well parametrized for the interactions associated with graphite; thus, the results presented here should be taken with care. Furthermore, during the simulations, the

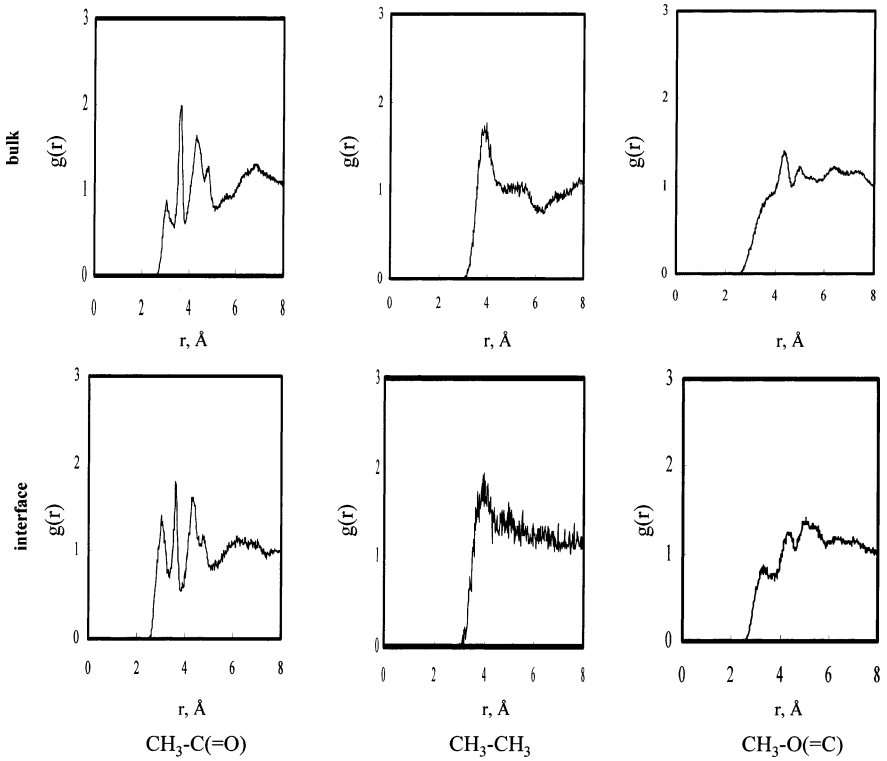


**Figure 11.** The pair distribution functions for the methyl carbon of Li-PDC both in bulk and at interface with graphite: the methyl carbon-the carbonyl carbon, the methyl carbon-the methyl carbon, and the methyl carbon-the carbonyl oxygen. See text for detail.

graphite carbons were neutral. In reality, the electrode is negatively charged during the recharge of a Li-ion secondary battery. Thus, the simulations in this study are only to examine the basic nature of the interactions between the graphite and the decomposition products.

## Conclusion

To understand the characteristics of the solvent decomposition products, the dilithium alkylene glycol dicarbonate products as the major components of SEI films, in different Li-ion secondary battery electrolytes, two theoretical protocols have been utilized: DFT calculations of solvent decomposition in solution and MD simulations of the decomposition compounds and graphite. Based on our work, the following points can be made. First, in the gas phase, the first electron reduction for the cyclic carbonates and the linear carbonates is found to be exothermic and endothermic, respectively, while the second electron reduction is endothermic for the cyclic carbonates. On the contrary, in solution both first and second electron reductions are exothermic for all the compounds, though the second electron reduction energies could not be obtained for the linear carbonates. In general, the cyclic carbonates are more likely to undergo reduction than the linear counterparts. Among the cyclic carbonates, VC is most susceptible to a two-electron reduction, possibly one of the characteristics as an additive for SEI film formation, though polymerization of the one-electron reduction product is likely to proceed in parallel for building a foundation for SEI film. Even in the presence of a lithium ion, the above finding seems unaltered. Still, our calculations warrant further study on the effect of the VC's two-electron reduction on SEI film formation. Among the cyclic carbonate solvents, EC and PC, or the linear carbonate solvents, DMC, EMC, and DEC, no significant difference was found in their reduction reaction thermodynamics.

As to the sharp contrast in the cycling behavior between the EC- and the PC-based electrolytes, our MD simulations have clearly shown the difference between the two decomposition products in the physical properties and the interactions with graphite which may contribute to the behaviors in the first cycling. The EC-based electrolyte is more likely to form a firm and adhesive SEI film, that is less soluble to the electrolyte, possibly more quickly than the PC-based electrolyte whose decomposition product is less dense and more soluble to the solvent, built slowly on the graphite surface due to the methyl group, which confirms Aurbach's model.[64] This difference should affect the performance not only in SEI film formation but also in the battery calendar cycle. Furthermore, the EC-based decomposition product has a stronger interaction with graphite than the PC counterpart whose methyl group seems to prevent good adhesion to the graphite surface. The structural effect of graphite on the decomposition molecule may be at work. Few studies have been reported on the difference in the physical properties of the SEI film in various electrolytes, and more detailed experimental study is in order.

Regarding the sticky-finger model proposed by Ein-Eli,[65] our calculations of adhesive energies show a small but consistent difference between the EC- and PC-based decomposition products. However, the sticky-finger model is based on the electrostatic interactions between the negatively charged graphite surface and the neutral decomposition compounds, while our system is all neutral. Hence, our calculations show the EC-based decomposition product has a favorable interaction with graphite even without strong electrostatic interactions. Our results on the bulk properties of Li-EDC and Li-PDC are also in line with Ein-Eli's model in terms of the compactness of the film.[65]

The methyl group of PC and its decomposition product seems to play a critical role in the physical properties, and its effect therefore has many implications for the SEI film: a lower molecular packing and thus a more brittle film, a higher solubility to the electrolyte, the extra molecular process needed for building up an SEI film, and a smaller adhesion to the

graphite surface, due to the interaction between the methyl group and graphite.

However, there are a number of reports suggesting the solvent co-intercalation into the graphite as the first step of SEI film formation as well[30−33] which may illegitimatize the model study such as the current work where the physical properties of solvent decomposition products are discussed in the different cycle behaviors between solvents. However, a recent study has shown that Li intercalation was made possible even in PC, but at a higher salt concentration, and a stable film was formed on graphite without exfoliation.[100] This study demonstrates that an SEI film can be formed without co-intercalation of PC when a high salt concentration is used. An earlier report indicated that a co-intercalation of PC always caused exfoliation of graphite.[31] This is one example showing a complexity of SEI film formation for which no single model is widely accepted, and computer modeling work such as the current study can be helpful in sorting out different possible causes.

In this study, we found significant differences in the thermodynamic properties between the solvent decomposition products of EC and PC, based on our MD simulations. These differences certainly contribute to the behaviors of electrolytes during the first recharge cycle. However, a real SEI film is far more complex than the current system, including inorganic as well as organic components with salt anions, and also Li-PDC may not be formed directly on the graphite surface. Also, a discussion on the kinetic aspect of SEI film formation was not presented in this study since our focus is on the thermodynamic element of SEI film. Yet, study of the model compounds such as this work can reveal an important insight into the difference among solvents in order to understand the stability of SEI film based on the molecular structure, which is difficult to probe experimentally. Thus, this study should be regarded as a model study rather than a simulation of a real system. The difference among the linear carbonates will be the subject of a forthcoming paper.

**Acknowledgment.** The author is indebted to Drs. Hitoshi Ota, Makoto Ue, Shinichiro Nakamura, and Katsuya Kanda of Mitsubishi Chemical Science and Technology Research Center, Inc., for the comments and the discussions.

**Supporting Information Available:** Table of optimized geometries for the solvent molecules examined and table of absolute energies for the solvent molecules examined. This material is available free of charge via the Internet at http://pubs.acs.org.

## References and Notes

(1) Besenhard, J. O.; Fritz, H. P. *J. Electrochem. Soc.* **1974**, *3*, 329.
(2) Eichinger, G. *J. Electrochem. Soc.* **1976**, *74*, 183.
(3) Peled, E. *J. Electrochem. Soc.* **1979**, *126*, 2047.
(4) Koch, V. R. *J. Electrochem. Soc.* **1979**, *126*, 181.
(5) Peled, E. In *Lithium Batteries*; Gbano, J. P., Ed.; Academic Press: New York, 1983; p 43.
(6) Aurbach, D.; Daroux, M. L.; Faguy, P. W.; Yeager, E. *J. Electrochem. Soc.* **1987**, *134*, 1611.
(7) Shu, Z. X.; McMillan, R. S.; Murray, J. J. *J. Electrochem. Soc.* **1993**, *140*, 922.
(8) Peled, E.; Tow, D. B.; Melman, A.; Gerenrot, E.; Lavi, Y.; Ronsenberg, Y. In *Lithium Batteries*; Doddapaneni, N., Langrebe, A. P., Eds.; The Electrochemical Society Proceedings Series, Vol. PV 94-4; Electrochemical Society: Pennington, NJ, 1994; p 177.
(9) Dominey, L. A. In *Lithium Batteries*: *New Materials, Development and Perspectives*; Pistoia, G., Ed.; Elsevier: New York, 1994; p 137.
(10) Dahn, J. R.; Sleigh, A. K.; Shi, H.; Way, B. M.; Weydanz, W. J.; Reimers, J. N.; Zhong, Q. In *Lithium Batteries*: *New Materials, Development and Perspectives*; Pistoia, G., Ed.; Elsevier: New York, 1994; p 22.
(11) Aurbach, D.; Ein-Eli, Y.; Chuid, O.; Carmeli, Y.; Babai, M.; Yamin, H. *J. Electrochem. Soc.* **1994**, *141*, 603.
(12) Aurbach, D.; Ein-Eli, Y. *J. Electrochem. Soc.* **1995**, *142*, 1746.
(13) Aurbach, D.; Ein-Eli, Y.; Markovsky, B.; Zaban, A.; Luski, S.; Carmeli, Y.; Yamin, H. *J. Electrochem. Soc.* **1995**, *142*, 2882.
(14) Bsesenhard, J. O.; Winter, M.; Yang, J.; Biberacher, W. *J. Power Sources* **1995**, *54*, 28.
(15) Inaba, M.; Shiroma, Z.; Ogumi, Z.; Abe, T.; Mizutani, Y.; Asano, M. *Chem. Lett.* **1995**, 661.
(16) Aurbach, D.; Markovsky, B.; Shecher, A.; Ein-Eli, Y. *Chem. Lett.* **1996**, *143*, 3809.
(17) Naji, A.; Ghanbaja, J.; Humbert, B.; Willmann, P.; Billaud, B. *J. Power Sources* **1996**, *63*, 33.
(18) Mori, S.; Asahina, H.; Suzuki, H.; Yonei, A.; Yasukawa, E. *Ext. Abstr. 8th Int. Meet. Lithium Batteries* **1996**, 40.
(19) Hirasawa, K. A.; Sato, T.; Asahina, H.; Yomaguchi, S.; Mori, S. *J. Electrochem. Soc.* **1997**, *144*, L81.
(20) Matsuura, Y.; Wang, S.; Mondori, J. *J. Electrochem. Soc.* **1995**, *142*, 2914.
(21) Aurbach, D.; Markovsky, B.; Schechter, A.; Ein-Eli, Y.; Cohen, H. *J. Electrochem. Soc.* **1996**, *143*, 3809.
(22) Naji, A.; Ghanbaja, J.; Willmann, P.; Humbert, B.; Billaud, D. *J. Power Sources* **1996**, *62*, 141.
(23) Yazami, R.; Guerard, D. *J. Power Sources* **1993**, *43*−*44*, 39.
(24) Winter, M.; Besenhard, J. O.; Spahr, M. E.; Novak, P. A*dv. Mater.* **1998**, *10*, 725.
(25) Endo, E.; Tanaka, K.; Sekai, K. *J. Electrochem. Soc.* **2000**, *147*, 4029.
(26) Aurbach, D. *J. Power Sources* **2000**, *89*, 206.
(27) Peled, E.; Golodnitsky, D.; Ardel, G.; Menachem, C.; Bar-Tow, D.; Eshkenazy, V. *Mater. Res. Soc. Symp.* **1995**, *393*, 209.
(28) Peled, E.; Menachem, C.; Bar-Tow, D.; Melman, A. *J. Electrochem. Soc.* **1996**, *143*, L4.
(29) Ota, H.; Akai, T.; Namita, H.; Yamaguchi, S.; Nomura, M. *J. Power Sources* **2003**, *119*, 567.
(30) Abe, T.; Kawabata, N.; Mizutani, Y.; Inaba, M.; Oguni, Z. *J. Electrochem. Soc.* **2003**, *150*, A257.
(31) Jeong, S.-K.; Inaba, M.; Mogi, R.; Iriyama, Y.; Abe, T.; Ogumi, Z. *Langmuir* **2001**, *17*, 8281.
(32) Jeong, S.-K.; Inaba, M.; Iriyama, Y.; Abe, A.; Ogumi, Z. *J. Power Sources* **2003**, *119*−*121*, 555.
(33) Winter, M.; Besenhard, J. O.; Spahr, M. E.; Novák, P. *Adv. Mater.* **1998**, *10*, 725.
(34) Fong, R.; von Sacken, U.; Dahn, J. R. *Adv. Mater*. **1990**, *137*, 2009.
(35) Peled, E.; Golodnitsky, D.; Pencier, J. In *Handbook of Battery Materials*; Besenhard, J. O., Ed.; Wiley-VCH: New York, 1999; p 419.
(36) Kohs, W.; Santner, H. J.; Hofer, F.; Schrottner, H.; Doninger, J.; Barsukov, I.; Buqa, H.; Albering, J. H.; Moller, K.-C.; Besenhard, J. O.; Winter, M. *J. Power Sources* **2003**, *119*, 528.
(37) Yoshio, M.; Nakamura, H.; Yoshitake, H.; Tanaka, S. U.S. Patent 5,681,669, Oct 28, 1997.
(38) Shu, Z. X.; McMillan, R. S.; Murray, J. J.; Davidson, I. J. *J. Electrochem. Soc.* **1995**, *142*, L161.
(39) Shu, Z. X.; McMillan, R. S.; Murray, J. J.; Davidson, I. J. *J. Electrochem. Soc.* **1996**, *143*, 2230.
(40) Ein-Eli, Y.; Thomas, S. R.; Koch, V. R. *J. Electrochem. Soc.* **1997**, *142*, 1159.
(41) Wrodnigg, G. H.; Besenhard, J. O.; Winter, M. *J. Electrochem. Soc.* **1999**, *146*, 470.
(42) Foster, D. L.; Behl, W. K.; Wolfenstine, J. *J. Power Resources* **2000**, *85*, 299.
(43) Moller, K.-C.; Santner, H. J.; Kern, W.; Yamaguchi, S.; Besenhard, J. O.; Winter, M. *J. Power Sources* **2003**, *119*, 561.
(44) Vetter, J.; Novak, P. *J. Power Sources* **2003**, *119*, 338.
(45) Yoshitake, H.; Abe, K.; Kitakura, T.; Gong, J. B.; Lee, Y. S.; Nakamura, H.; Yoshio, M. *Chem. Lett.* **2003**, *32*, 134.
(46) Ota, H.; Akai, T.; Kotato, M.; Yamaguchi, S. *Abstracts of the International Meeting on Lithium Batteries*, Monterey, 2002; 335.
(47) Zhang, X.; Pugh, J. K.; Ross, P. N. *Abstracts of the Electrochemical Society Meeting*, Toronto, 2000; Electrochemical Society: Pennington, NJ, 2000; *2000-1*, 112.
(48) Zhang, X.; Pugh, J. K.;. Ross, N. *Abstracts of the Electrochemical Society Meeting*, Phoenix, 2000; Electrochemical Society: Pennington, NJ, 2000; *2000-2*, 342.
(49) Zhang, X.; Pugh, J. K.; Ross, P. N. *J. Electrochem. Soc.* **2001**, *148*, E183.
(50) Wang, Y.; Balbuena, P. B. *J. Phys. Chem. B* **2002**, *106*, 4486.
(51) Aurbach, D.; Gamolsky, K.; Markovsky, B.; Gofer, Y.; Schmidt, M.; Heider, U. *Electrochim. Acta* **2002**, *47*, 1423.
(52) Ota, H. Ph.D. Thesis, Kyushu University, Fukuoka, Japan, 2003.
(53) Dey, A. N.; Sullivan, B. P. *J. Electrochem. Soc.* **1970**, *117*, 222.
(54) Bar-Tow, D.; Peled, E.; Burstein, L. *J. Electrochem. Soc*. **1999**, *146*, 824.

(55) Aurbach, D.; Moshkovich, M.; Cohen, Y.; Schechter, A. *Langmuir* **1999**, *15*, 2947.
(56) Schechter, A.; Aurbach, D.; Cohen, H. *Langmuir* **1999**, *15*, 3334.
(57) Aurbach, D. J. *Power Sources* **2000**, *89*, 206.
(58) Yang, C. R.; Wang, Y. Y.; Wan, C. C. *J. Power Sources* **1998**, *72*, 66.
(59) Aurbach, D.; Ein-Eli, Y.; Zaban, A. *J. Electrochem. Soc.* **1994**, *141*, L1.
(60) Naji, A.; Ghanbaja, J.; Humbert, B.; Willmann, P.; Billaud, D. *J. Power Sources* **1996**, *63*, 33.
(61) Aurbach, D.; Levi, M. D.; Levi, E.; Schechter, A. *J. Phys. Chem. B* **1997**, *101*, 2195.
(62) Li, T.; Balbuena, P. B. *Chem. Phys. Lett*. **2000**, *317*, 422.
(63) Wang, Y.; Nakamura, S.; Ue, M.; Balbuena, P. B. *J. Am. Chem. Soc.* **2001**, *123*, 11708.
(64) Aurbach, D.; Zinigrad, E.; Cohen, Y.; Teller, H. *Solid State Ionics* **2002**, *148*, 405.
(65) Ein-Eli, Y. *Electrochem. Solid-State Lett.* **1999**, *2*, 212.
(66) Inaba, M.; Tomiyasu, H.; Tasaka, A.; Jeong, S.-K.; Iriyama, Y.; Abe, T.; Ogumi, Z. *Abstracts of the Electrochemical Society Meeting*, Orlando, 2003; Electrochemical Society: Pennington, NJ, 2003; *2003-2*, 406.
(67) Smart, M. C.; Ratnakumar, B. V.; Ryan-Mowrey, V. S.; Surampudi, S.; Prakash, G. K. S.; Cheung, J. H. I. *J. Power Sources* **2003**, *119*−*211*, 359.
(68) Chung, G.-C. *J. Power Sources* **2002**, *104* (1), 7.
(69) Aurbach, D.; Ein-Eli, Y.; Chusid, O. Y.; Babai, M.; Carmeli, Y.; Yamin, H. *J. Electrochem. Soc.* **1994**, *141*, 603.
(70) Foresman, J. B.; Frisch, A. E. In *Exploring Chemistry by Electronic Structure Theory*, 2nd ed.; Gaussian, Inc.: Pittsburgh, 1999; p 194.
(71) *Handbook of Chemistry and Physics*, 79th ed.; Lide, D. R., Ed.; CRC Press: New York, 1998−1999.
(72) Barone, V.; Cossi, M. *J. Phys. Chem. A* **1998**, *102*, 1995.
(73) Keeffe, J. R.; Gronert, S.; Colvin, M. E.; Tran, N. L. *J. Am. Chem. Soc.* **2003**, *125* (38), 11730.
(74) Sillanpaeae, A. J.; Aksela, R.; Laasonen, K. *Phys. Chem. Chem. Phys*. **2003**, *5* (16), 3382.
(75) Krossing, I.; Bihlmeier, A.; Raabe, I.; Trapp, N. *Angew. Chem., Int. Ed*. **2003**, *42* (13), 1531.
(76) Baik, M.-H.; Ziegler, T.; Schauer, C. K. *J. Am. Chem. Soc*. **2000**, *122* (38), 9143.
(77) Linden, D. *Handbook of Batteries*, 2nd ed.; McGraw-Hill: New York, 1995; p 36.14.
(78) For weight-averaged dielectric constants, see the following reference: Becker, R. J. *J. Appl. Phys.* **1987**, *61* (3), 1123.
(79) Frisch, M. J.; Trucks, G. W.; Schlegel, H. B.; Gill, P. M. W.; Johnson, B. G.; Robb, M. A.; Cheeseman, J. R.; Keith, T.; Peterson, G. A.; Montgomery, J. A.; Raghavachari, K.; Al-Lahoresman, M. A.; Zakrzewski, V. G.; Ortiz, J. V.; Foresman, J. B.; Peng, C. Y.; Ayala, P. Y.; Cheng, W.; Wong, M. W.; Andres, J. L.; Replogle, E. S.; Gomperts, R.; Martin, R. L.; Fox, D. J.; Binkley, J. S.; Defrees, D. J.; Baker, J.; Stewart, J. P.; Head-Gordon, M.; Gonzalez, C. Pople, J. A. *Gaussian 98*, Revision A.1; Gaussian Inc.: Pittsburgh, 1998.
(80) *Cerius*$^2$, Version 4.0 Modeling Environment; Accelrys: San Diego, 2002.
(81) Sun, H. *J. Phys. Chem. B* **1998**, *102*, 7338.
(82) Ewald, P. *Ann. Phys*. **1921**, *64*, 253.
(83) van Gunsteren, W. F.; Berendsen, H. J. C. *Mol. Phys.* **1977**, *34*, 1311.
(84) Kinoshita, K. *Carbon Electrochemical and Physicochemical Properties*; John Wiley: New York, 1988; p 20.
(85) Blint, R. J. *J. Electrochem. Soc.* **1995**, *142*, 696.
(86) Blint, R. J. *J. Electrochem. Soc.* **1997**, *144*, 787.
(87) Wang, Y.; Nakamura, S.; Tasaki, K.; Balbuena, P. B. *J. Am. Chem. Soc.* **2002**, *124*, 4408.
(88) Wang, Y.; Balbuena, P. B. *J. Phys. Chem. A* **2001**, *105*, 9972.
(89) Matsuda, S.; Asada, T.; Kitaura, K. *J. Electrochem. Soc*. **2000**, *147*, 1695.
(90) Han, Y.-K.; Sang, U.; Ok, J.-H.; Cho, J.-J.; Kim, H.-J. *Chem. Phys. Lett*. **2002**, *360*, 359.
(91) Wang, Y.; Balbuena, P. B. *J. Phys. Chem. B* **2003**, *107*, 5503.
(92) Wang, Y.; Balbuena, P. B. *J. Phys. Chem. A* **2002**, *106*, 9585.
(93) Arai, J.; Katayama, H.; Akahoshi, H. *J. Electrochem. Soc.* **2002**, *149* (2), A217.
(94) Barthel, J.; Gores, H. J. In *Handbook of Battery Materials*; Besenhard, J. O., Ed.; Wiley-VCH: New York, 1999; p 460.
(95) Hong, C. S.; Waksiak, R.; Finston, H.; Fried, V. *J. Chem. Eng. Data* **1982**, *27*, 146.
(96) Steele, W. V.; Chirico, R. D.; Knipmeyer, S. E.; Nguyen, A. *J. Chem. Eng. Data* **1997**, *42*, 1008.
(97) Botte, G. G.; Bauer, T. J. *J. Power Sources* **2003**, *119*, 815.
(98) Månsson, M. *J. Chem. Thermodyn*. **1972**, *4*, 865.
(99) Bar-Tow, D.; Peled, E.; Burstein, L. *J. Electrochem. Soc*. **1999**, *146* (3), 824.
(100) Jeong, S.-K.; Inaba, M.; Iriyama, Y.; Abe, T.; Ogumi, Z. *Electrochem. Solid-State Lett.* **2003**, *6* (1), A13.